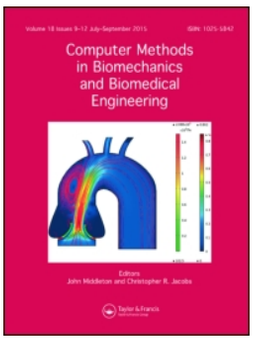

Taylor & Francis
Taylor & Francis Group

Computer Methods in Biomechanics and Biomedical Engineering

ISSN: 1025-5842 (Print) 1476-8259 (Online) Journal homepage: http://www.tandfonline.com/loi/gcmb20

Error reduction in the finite helical axis for knee kinematics

Emily L. Bishop, Jessica C. Küpper, Ingrid R. Fjeld, Gregor Kuntze & Janet L. Ronsky

To cite this article: Emily L. Bishop, Jessica C. Küpper, Ingrid R. Fjeld, Gregor Kuntze & Janet L. Ronsky (2018) Error reduction in the finite helical axis for knee kinematics, Computer Methods in Biomechanics and Biomedical Engineering, 21:2, 186-193, DOI: 10.1080/10255842.2018.1435780

To link to this article: https://doi.org/10.1080/10255842.2018.1435780

COMPUTER METHODS IN BIOMECHANICS AND BIOMEDICAL ENGINEERING, 2018
VOL. 21, NO. 2, 186–193
https://doi.org/10.1080/10255842.2018.1435780

Taylor & Francis
Taylor & Francis Group

Error reduction in the finite helical axis for knee kinematics

Emily L. Bishop[a,b,c], Jessica C. Küpper[a,b], Ingrid R. Fjeld[a,b], Gregor Kuntze[b] and Janet L. Ronsky[a,b]

[a]Department of Mechanical and Manufacturing Engineering, Schulich School of Engineering, University of Calgary, Calgary, Canada; [b]McCaig Institute for Bone and Joint Health, Cumming School of Medicine, University of Calgary, Calgary, Canada; [c]Biomedical Engineering Graduate Program, University of Calgary, Calgary, Canada

ABSTRACT

Traditionally the FHA is calculated stepwise between data points (sFHA), requiring down sampling to achieve a sufficiently large step size to minimize error. This paper proposes an alternate FHA calculation approach (rFHA), using a unique reference position to reduce error associated with small rotation angles. This study demonstrated error reduction using the rFHA approach relative to the sFHA approach. Furthermore, the rFHA in the femur is defined at each time point providing a continuous representation of joint motion. These characteristics enable the rFHA to quantify small differences in knee joint motion, providing an excellent measure to quantify knee joint stability.

ARTICLE HISTORY
Received 2 April 2017
Accepted 29 January 2018

KEYWORDS
Finite helical axis; error reduction; knee kinematics; joint stability

1. Introduction

The finite helical axis (FHA) is an effective approach to describe knee joint motion by defining a single axis about which the femur and tibia articulate. Thereby, tibial motion is described as a rotation and translation about a moving three-dimensional (3D) FHA embedded in the femur. Changes in knee joint kinematics may be quantified using resultant variables that describe the position and movement of the FHA throughout a dynamic task. An advantage of the FHA is its independence of the local coordinate system (LCS) definition and the order of translations and rotations (Blankevoort et al. 1990). Consequently, the FHA is not constrained to three pre-defined planes of motion, as it is with Cardan/Euler or Joint Coordinate System approaches (Grood & Suntay 1983). Rather, the FHA is defined in 3D space based on the relative movement of the femur and tibia throughout a dynamic task. Therefore, the FHA provides meaningful information regarding the axis of rotation and changes in relative segment orientations. This information is particularly important when investigating the consequences of anterior cruciate ligament (ACL) rupture. However, limitations of the FHA include the sensitivity to errors at small rotations (Woltring et al. 1985), and the lack of a consistent set of variables to quantify the FHA behavior (Blankevoort et al. 1988; Dennis et al. 2005; Sheehan 2007).

Typically, the FHA is calculated in a stepwise manner (sFHA), using down sampling to optimize step sizes as a means to minimize computational error. However, FHA resolution decreases as a result. This paper proposes an alternate approach to reduce error while maintaining FHA resolution. Specifically, a reference position (rFHA) approach is implemented to calculate the FHA at each data point between the position of interest and a stationary reference position. This approach retains all data points by removing the need for down sampling and maintains the requirement for large step sizes to minimize error. Therefore, with respect to the knee joint, both the sFHA and rFHA compute an axis about which the tibia rotates with respect to the femur between consecutive time points. However, unlike the sFHA that refers to the previous data point, the rFHA uses information from the same stationary segment orientation (reference position) for each rFHA iteration.

The objective of this research was to assess the use of the reference position (rFHA) approach to enhance temporal resolution, while minimizing computational errors, and to identify a set of FHA outcome variables that may be suitable to fully describe the FHA in 3D space. The requirements of the rFHA approach with respect to the knee joint were to (1) minimize error to enable detection of small differences in knee joint motion; (2) provide a continuous representation of knee joint motion throughout a dynamic task; and (3) provide a set of FHA outcome variables that allow for a comprehensive description of the FHA in 3D space. Error reduction was assessed by comparing factors of error between the rFHA and sFHA

CONTACT Emily L. Bishop elbishop@ucalgary.ca

approaches. Effective error management strategies to enable high FHA temporal resolution and standardized FHA outcome measures may support the assessment of the injured knee joint and enable data comparisons across studies.

2. Materials and methods

2.1. FHA error analysis

An error analysis was performed based on Woltring et al. (1985) to estimate FHA error as a function of rotation angle. The factors of error (FE) are defined as the portions of the error equation for a given FHA parameter that are a function of rotation angle. The FE were calculated at flexion step sizes of 0°, 5°, 10°, 50°, and 70°. Errors in rotation angle and translation along the axis (t) are not affected by rotation angle (Woltring et al., 1985, Equation 25). For the unit vector (**n**), error is inversely proportional to the angle by a factor (FE_n), and a constant (C) dependent on the system and landmarks (i.e. unaffected by angle):

$$\sigma_{\hat{n}}^2 \cong C * \frac{1}{\left(\sin\frac{1}{2}\theta\right)^2} = C * FE_n \tag{1}$$

where $\sigma_{\hat{n}}^2$ = total variance in $\hat{n}$ (estimated parameter **n**), θ is rotation angle, and:

$$C = \frac{\sigma^2}{m\rho^2} \tag{2}$$

where σ is error distribution (related to the measurement system), m is number of landmarks, and ρ is effective landmark distribution radius (root mean square (RMS) distance of landmarks to an arbitrary line through x, the mean position of the landmarks).

For a point on axis (**s**) location, error varies inversely with angle (θ) by three FE:

$$\begin{aligned}\sigma_{\hat{s}_n}^2 &\cong C_1 \sin^{-2}\frac{1}{2}\theta\left(1 + C_2\frac{1}{4}\tan^{-2}\frac{1}{2}\theta + C_3\frac{1}{2}\cos^{-2}\frac{1}{2}\theta\right)\\ &= C_1\left(\sin\frac{1}{2}\theta\right)^{-2} + C_1C_2\left(\sin\frac{1}{2}\theta\right)^{-2}\frac{1}{4}\left(\tan\frac{1}{2}\theta\right)^{-2}\\ &\quad + C_1C_3\left(\sin\frac{1}{2}\theta\right)^{-2}\frac{1}{2}\left(\cos\frac{1}{2}\theta\right)^{-2}\\ &= C_1FE_{s1} + C_1C_2FE_{s2} + C_1C_3FE_{s3}\end{aligned} \tag{3}$$

where $\sigma_{\hat{s}_n}^2$ = total variance in $\hat{s}$ (estimated parameter **s**), and

$$C_1 = \frac{\sigma^2}{m} \tag{4}$$

$$C_2 = \frac{t^2}{\rho^2} \tag{5}$$

$$C_3 = \frac{|s-p|^2}{\rho^2} \tag{6}$$

where t is the translation along the axis, p is the midpoint on the translation vector from point 1 to point 2, and s is the projection of p onto the helical axis.

The factor of error in the unit vector multiplier (FEn), and the first (FEs1), second (FEs2), and third (FEs3) factors of error in the point on the axis multiplier were calculated and compared for the rFHA and sFHA approaches.

2.2. FHA outcome variable assessment

To experimentally calculate and quantify the rFHA and sFHA, one healthy female (23 years, BMI 22.1 kg/m) signed informed consent and participated in this Conjoint Health Research Ethics Board approved study. Testing was performed in two stages to measure and locate the FHA in the subject's joint. Kinematic FHA variables were obtained as the subject performed two tasks. Knee joint geometry was quantified using MR imaging and a custom knee loading apparatus (KLA, Küpper et al., 2013).

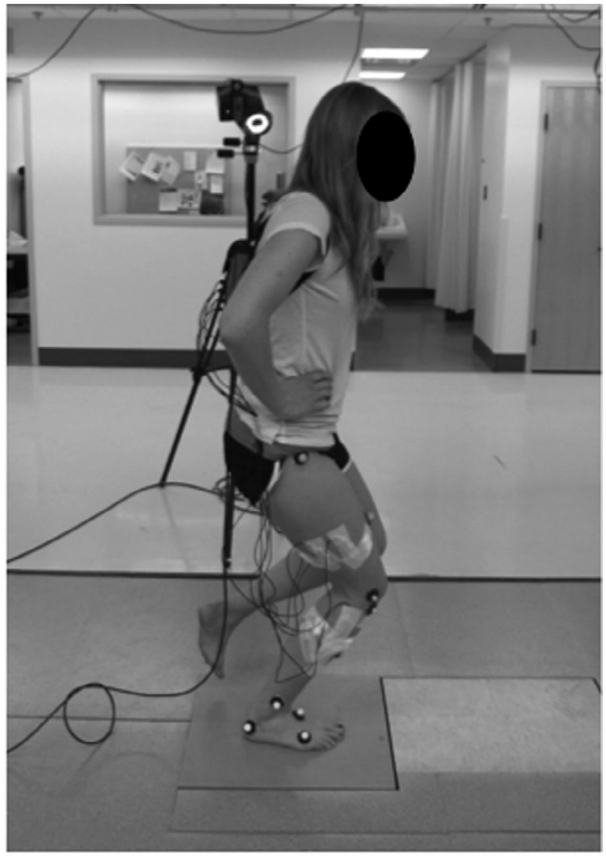

Figure 1. Participant performing the single-legged squat task.

2.2.1. Kinematic testing

The participant performed a seated leg swing (90° hip and knee flexion with foot clear of the floor, completing five swings to full extension (0°) and back to 90° flexion), and a single leg squat (knee flexed from full extension to ~60° flexion and back, Figure 1). Task pace was regulated with a metronome (60 beats/min). Kinematic data (3D) were acquired using an eight-camera high-speed video motion capture system (120 Hz; capture volume 1.3 × 1.2 × 1.2 m^3) and EVaRT 4.0 software (Motion Analysis Corporation, Santa Rosa, CA) with nine skin-mounted spherical reflective markers (Ø = 20 mm, Figure 2). Markers were placed in a manner to optimize marker distribution on each limb segment, while avoiding areas that would have large soft tissue movement relative to the bone to minimize error due to skin movement artefact. Two neutral trials were obtained (3s) with four additional markers for coordinate transformations to: (1) provide an rFHA reference position (sitting with hip and knee at 90°), and (2) provide a linkage between the motion analysis global coordinate system (GCS) and MR image coordinate system (ICS) [supine neutral trial (30° knee flexion)].

Marker motions were tracked and filtered (fourth-order Butterworth, 10 Hz cut-off; Van den Bogert et al., 1996). Marker motion data were analysed using in-house FHA programs implemented in Matlab (v 6.5, The MathWorks Inc., Natick, MA).

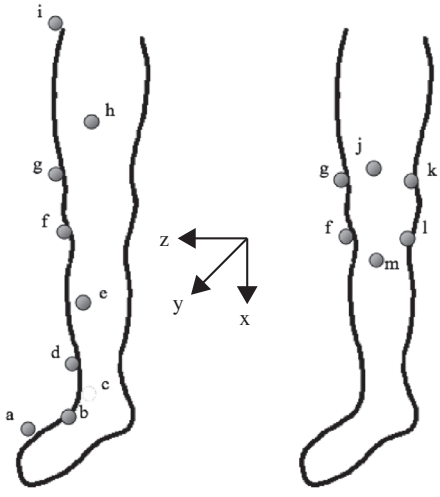

Figure 2. Segmental (left) and MR imaging (right) lower limb marker placement for 3D kinematic data collection. Segment markers were placed on the (a) fifth metatarsal, (b) supernavicular and (c) lateral calcaneus of the foot; (d) superior to the lateral mallelous, (e) anterior tibialis, and (f) proximal fibula of the shank; and (g) lateral femoral epicondyle, (h) anterior thigh and (i) greater trochanter for the thigh segment. An additional four markers, used with (g) and (f) for coordinate transformations between motion data and MR images, were placed around the knee on the (j) superior patella, (k) medial femoral epicondyle, (l) proximal medial tibia and (m) tibial tuberosity.

2.2.2. Magnetic resonance imaging

Directly after motion testing, the subject was imaged in a General Electric 3T MR scanner with a general-purpose flex coil (General Electric Healthcare, Waukesha, WI). A 3D Fiesta sequence (TR: 4.180 ms, TI: 0 ms, TE: 1.292 ms) produced sagittal images of the knee (0.781 mm × 0.781 mm × 2.6 mm resolution). Images were acquired at ~30° knee flexion (goniometer measured) with the KLA unloaded (anterior positioning frame, Kupper et al., 2013). Sagittal images of the knee were manually digitized using Amira 5.0 (FEI Visualization Science Group, Oregon U.S.A.; Figure 3). A 3D point cloud in the ICS was output for the tibia, femur and each marker.

2.2.3. Coordinate transformations

Kinematic data were transformed (Soderkvist & Wedin 1993) from the GCS to the ICS using the centroid coordinates of three markers located on the distal femur (Figure 3). Kinematic and MR data were then transformed into the LCS from the ICS. The LCS was defined using femoral geometry from MR images. To define the longitudinal axis (*x*-axis), an ellipse was fit to each axial slice of data points along the femoral shaft, and a least squares line was fit to the centroids of each ellipse. The mediolateral axis (*z*-axis) was based on the circular profile of the posterior femoral condyles (Churchill et al. 1998; Iwaki et al. 2000; Coughlin et al. 2003; Freeman & Pinskerova 2005). The anterior-posterior y-axis was obtained with the cross product of the z and x axes (positive y-axis in the anterior direction). To ensure orthogonality, the cross product of the y and z axes was calculated again. The coordinate system origin was located at the intersection of the x and z axes in the centre of the femoral facets. Two testers performed repeatability tests involving calculation of the LCS ten consecutive times on two separate occasions. Intra and inter-tester repeatability of the origin location in the midsagittal plane was 0.79 ± 0.42 mm and 0.85 ± 0.34 mm, respectively.

3D knee joint angles at each time point were calculated with rotation about the axes in the order z, y, x (Figure 2; Cole et al., 1993). A range of interest (ROI) for FHA evaluation (20–40° knee flexion, where full extension is 0°) was selected to examine 10° of motion on either side of 30° [approximate ACL slack/taut transition angle (Fleming et al. 1994) showing greatest anterior translation (Sakane et al. 1999)]. The 90° knee flexion reference position was selected to provide a simple and easy-to-position pose sufficiently far away from the ROI.

2.2.4. FHA calculation

The transformation matrix relating the position of the tibia with respect to the femur (T_{rel}) was calculated at each time point between the position of interest and a reference

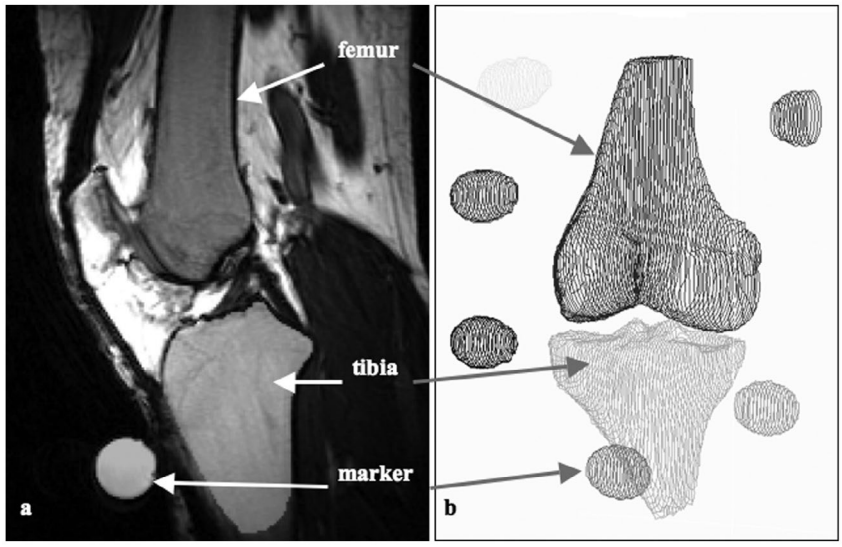

Figure 3. (a) Femur, tibia and six markers were digitized for each sagittal image slice at the trabecular/cortical bone interface, (b) resulting in a 3D volume of the femur, tibia and marker surfaces.

Notes: The orthogonal LCS longitudinal axis is the centre line of the femoral shaft. The medial/lateral axis is defined as a line connecting the centres of the posterior femoral condyles (positive z-axis defined as anatomical right). The origin is at the x and z axes intersection (relates to the centre of the femoral facets and is close to the femoral notch).

position (Soderkvist and Wedin, 1993). The resulting rotation matrix and translation vector were then used to calculate the FHA (Spoor & Veldpaus 1980). The rFHA was calculated using the reference position. The sFHA was calculated using a step size of 5° knee flexion (Blankevoort et al. 1988; van den Bogert et al. 2008).

2.2.5. FHA outcome variables

Seven parameters (three documented in literature, four novel proposed) were assessed: FHA location, translation, orientation, dispersion, path length, anterior/posterior (AP) excursion, and proximal/distal (PD) excursion. FHA location and orientation describe the position of the FHA within the joint. Specifically, FHA location is the FHA intersection at each time point with the knee midsagittal plane (LCS x-y plane; Figure 4; Blankevoort et al., 1990; Dennis et al., 2005; Dhaher and Francis, 2006; Jonsson and Kärrholm, 1994; van den Bogert et al., 2008; Westphal et al., 2013). FHA orientation is the angle between the FHA and the medial/lateral knee z-axis at each time point (Figure 4; Colle et al., 2012; Dhaher and Francis, 2006; Grip and Häger, 2013; Jonsson and Kärrholm, 1994; Kessler et al., 2007; Morishige et al., 2010; van den Bogert et al., 2008).

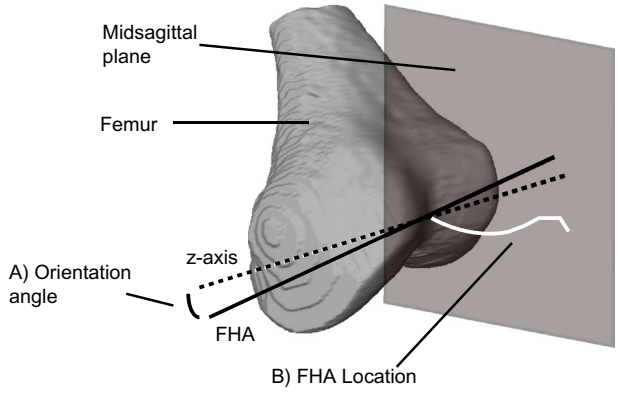

Figure 4. Schematic of (A) FHA orientation angle, defined as the angle of the FHA at each time point with the mediolateral z-axis of the LCS, and (B) FHA location, defined as the intersection point of the FHA at each time point with the midsagittal plane of the knee, resulting in a trace (shown in white) of the FHA path of travel during joint motion.

FHA translation, dispersion, path length, and AP/PD excursion describe movement of the FHA throughout a dynamic task. FHA translation is the vector summation of the transformation matrix translation components along the FHA unit vector at each time point (Spoor & Veldpaus 1980; Shiavi et al. 1987; Grip & Häger 2013). FHA dispersion is the first novel proposed measure describing the spread of FHA rotation throughout a task, defined as the average angle between each individual axis and the mean FHA:

$$\theta_{d,\text{avg}} = \frac{\sum_{i=1}^{h} \cos^{-1}\left(\frac{(\vec{n}_{\text{mean}} \cdot \vec{n}_i)}{\sqrt{\vec{n}_{\text{mean}}^2} \times \sqrt{\vec{n}_i^2}}\right)}{h} \quad (7)$$

where $\theta_{d,\text{avg}}$ is the average dispersion angle, h is the number of FHA axes, $\vec{n}_i$ is the unit vector of the FHA at time t_i, and $\vec{n}_{mean}$ is the mean FHA unit vector.

FHA path length is the second novel proposed measure describing the length of the FHA location trace. It is the sum of Euclidean distances between each pair of consecutive FHA locations (x, y) (Equation 8). AP and PD excursion are the third and fourth novel proposed measures representing the AP/PD range covered by the FHA path (Equations 9 and 10).

$$\text{path} = \sum_{i=1}^{n-1} \sqrt{(x_{i+1} - x_i)^2 + (y_{i+1} - y_i)^2} \tag{8}$$

$$AP_{ex} = y_{max} - y_{min} \tag{9}$$

$$PD_{ex} = x_{max} - x_{min} \tag{10}$$

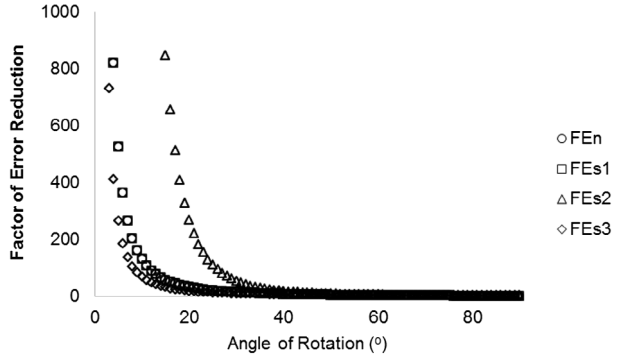

Figure 5. Factors of error in unit vector multiplier (FEn), and first (FEs1), second (FEs2), and third (FEs3) factors of error in point on axis multiplier with increasing angle of rotation.

3. Results

3.1. Error reduction of the FHA method

For the unit vector (**n**), the factor of error was 525.6 at the sFHA 5° step size, and decreased to 5.6–3.0 at the 50°–70° step sizes. For the point on axis location (s), each factor of error decreased with increasing step size by factors between 263.3 and 6.9×10^4 at 5° to 6.4–1.5 at 50° and 70° (Figure 5). Therefore, by using a reference position that was sufficiently far away from the ROI, the angle of rotation was increased, effectively reducing the error associated with FHA calculation.

Table 1. FHA results for the flexion (flex) and extension (ext) phases of the squat and swing tasks [mean (std)]. Calculations were performed using the rFHA and the sFHA with a 5° step size.

	Swing Ext		Swing Flex		Squat Ext		Squat Flex	
	rFHA	sFHA (5°)	rFHA	sFHA (5°)	rFHA	sFHA (5°)	rFHA	sFHA (5°)
Loc x (+ dist) (mm)	−6.79 (0.93)	6.02 (2.40)	−6.86 (0.73)	3.72 (5.15)	5.50 (0.44)	17.33 (8.92)	5.31 (0.59)	18.29 (9.00)
Loc y (+ ant) (mm)	30.53 (1.07)	30.26 (4.08)	30.81 (0.92)	27.63 (3.66)	29.79 (1.06)	37.88 (4.64)	30.39 (1.26)	24.27 (5.09)
Trans (mm)	3.07 (0.41)	3.72 (0.33)	−3.39 (0.92)	3.68 (0.84)	4.44 (0.38)	3.85 (0.32)	−4.27 (0.91)	3.86 (1.00)
Orient (deg)	20.69 (2.08)	16.92 (4.90)	19.03 (0.95)	20.49 (5.46)	9.94 (0.59)	7.69 (3.39)	10.51 (0.78)	12.49 (4.58)
Disp (deg)	2.04 (0.20)	8.71 (4.87)	1.55 (0.51)	9.83 (1.04)	0.78 (0.07)	6.84 (1.37)	1.19 (0.18)	9.78 (3.57)
Path (mm)	7.22 (1.85)	14.00 (10.34)	9.90 (1.90)	17.51 (12.08)	6.59 (0.17)	20.31 (19.39)	6.96 (1.12)	19.37 (15.65)
APex (mm)	3.80 (0.35)	5.92 (3.40)	3.30 (0.16)	4.98 (2.92)	3.56 (0.29)	6.50 (3.71)	3.96 (0.38)	7.56 (3.84)
PDex (mm)	3.31 (0.49)	4.48 (2.15)	3.19 (0.73)	7.01 (5.92)	1.55 (0.39)	9.90 (8.90)	1.55 (0.75)	8.00 (7.56)

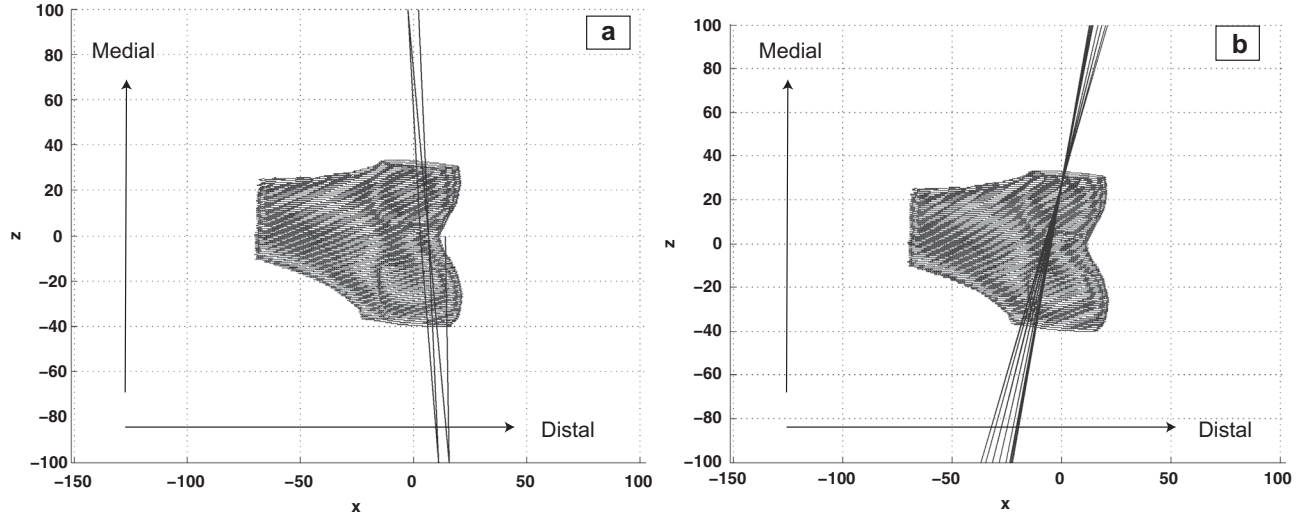

Figure 6. Plot of the FHA axes imposed on the subject's MR bone model throughout a swing movement, calculated using (a) sFHA 5° step size and (b) rFHA; coronal views shown.

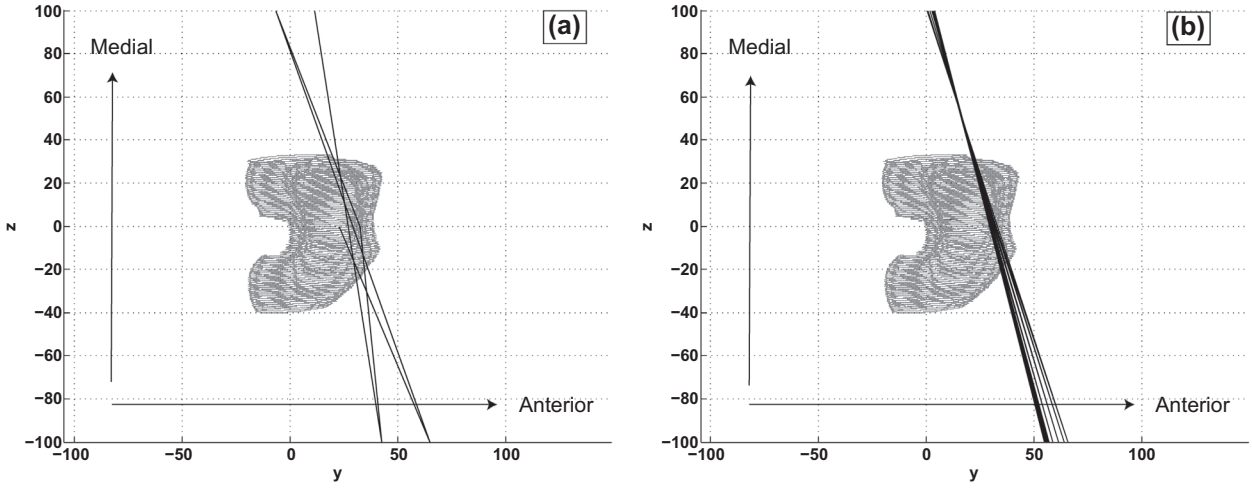

Figure 7. Plot of the FHA axes imposed on the subject's MR bone model throughout a swing movement, calculated using a sFHA 5° step size (a) and rFHA (b); axial views shown.

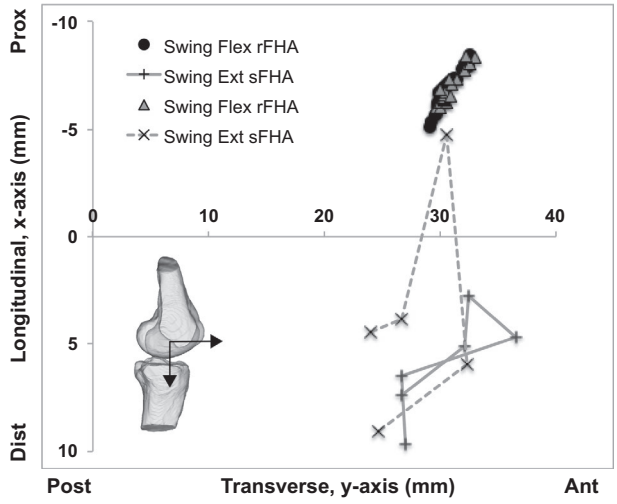

Figure 8. FHA location plot of FHA intersection point with the midsagittal plane of the knee throughout the ROI (20°–40°) for the flexion and extension phases of the swing task.
Note: Consecutive locations for the sFHA 5° step size are connected by a solid or dotted grey line.

3.2. FHA outcomes

The kinematic outcome variables obtained using sFHA and rFHA approaches displayed characteristic differences (Table 1). Figures 6 and 7 show each individual FHA plotted throughout the swing task. The rFHA provided a continuous representation of knee joint motion, while the sFHA showed lack of continuity. Highly fanned axes were observed for knee joint motion using the sFHA approach, which was reflected in higher values for dispersion. While orientation angle provided important information about the average angular position of the FHA, dispersion captured and quantified the angular spread in the individual axes from the mean axis.

The location path of the rFHA within the knee joint throughout the swing task (Figure 8) was continuous and fluid. In contrast, the path of the sFHA (Figure 8) was erratic and covered a larger area in both the longitudinal and transverse axes of the joint, resulting in higher values for path length. These observations highlight the discontinuous nature of the sFHA when using a 5° step size to reduce error associated with the calculation. The rFHA however, provided data for each degree resulting in a more complete picture of the path and range of motion of the FHA throughout the movement. While FHA location provided the average location of the FHA within the joint, path length tracked and captured the amount of FHA travel within the mid-sagittal plane of the knee joint, and AP and PD excursion provided even further information by isolating FHA movement in the AP and PD directions.

4. Discussion

This study reports a novel FHA calculation approach using a unique reference position to optimize temporal resolution while minimizing error in kinematic estimates. The findings of this investigation support the implementation of the rFHA approach based on the low computation errors observed. A set of seven standard FHA outcome variables are recommended to cover the main aspects of the location and motion of the FHA throughout a dynamic task. The proposed variables describe the 3D position of the FHA (i.e. position of the tibia with respect to the femur), and capture the magnitude and directionality of the axis motion in both the linear and angular sense, thereby providing a comprehensive assessment for change in joint kinematics due to injury.

The findings of the error propagation analysis indicated that the rFHA allows for a significant reduction in error relative to the sFHA, while maintaining the requirement for the FHA to be defined at each time point, thus providing a continuous representation of joint motion. The decreased rFHA error range (Figure 5) as the angle of rotation approached and exceeded 50° may be explained by the sensitivity of the FHA calculation to small rotation angles (Woltring et al. 1985) due to the requirement for the angle to be greater than 0° (Spoor and Veldpaus, 1980; Equation 38). For the point on axis location, the error is a summation of constants multiplied by FE and cannot be directly interpreted for overall scale in this theoretical analysis. In an experimental error simulation by Grip and Häger (2013), the largest absolute error in FHA position (with measurement and intra-marker distance noise added) was reduced from >60 mm using a 5° step size to ~11 and ~9 mm using the 50°–60° step size, respectively. From these results, it was demonstrated that the potential error introduced by a changing step size using the sFHA may be reduced by an order of magnitude using the rFHA approach.

In the case where a researcher is interested in how the FHA changes in an absolute sense (e.g. where the FHA is located relative to joint center for a given ROI), the sFHA with the largest possible step size may be the optimal choice, assuming error is sufficiently minimized. For the same ROI, this technique can be used to analyze changes in the FHA throughout a motion (i.e. overall movement of FHA) and to determine whether an increase in joint motion is observed between two groups (e.g. path length). However, it is important to be aware that when using the sFHA, the influence of error may mask some of these features and show a less detailed picture of the relative change in axis location throughout a movement.

The underlying assumption with this motion analysis based measure is that the markers represent the motion of the underlying bone. However, skin motion artefacts are a limitation of this assumption and introduce some error (Peters et al., 2010). Interpretation of the rFHA must take into account the reference position, as it will affect the overall location of the FHA. Furthermore, the reference position should be standardized to allow for future data comparisons. As shown in the experimental validation of this study, the sFHA and rFHA approaches yielded different results for the same set of data. This result was expected, since the two approaches are fundamentally different (i.e. position 1 is different for each approach). This study used data from a single subject to experimentally calculate and quantify the rFHA and sFHA for the purposes of demonstrating these two approaches. The results presented are not intended to be used to determine statistical differences between methods or dynamic tasks.

The rFHA in the femur is defined at each time point and provides a continuous representation of the FHA. The error reduction provided with the rFHA approach, paired with the capability of providing a continuous representation of joint motion enables the rFHA approach to quantify small differences in knee joint motion that might otherwise be missed. The rFHA approach meets the requirements for future research aiming to determine differences between healthy and injured (ACLD) knee motion over time during dynamic tasks. For example, the rFHA could be used to compare knee joint motion within an individual between limbs, and between tasks to identify changes due to an injury or intervention. In particular, assessment of joint stability may be done with the rFHA approach. Knees can also be compared within a subject over time, using the same reference position, as it gives a relative measure of knee motion. A standardized set of FHA measures have been proposed with the aims of more completely describing the FHA, and highlighting its potential as a tool in both research and clinical settings.

Acknowledgements

The authors would like to acknowledge funding support from the Natural Sciences and Engineering Research Council of Canada (NSERC), Alberta Innovates Technology Futures (AITF), the Canadian Institutes of Health Research (CIHR), and Alberta Innovates Health Solutions (AIHS). Additionally, the authors would like to acknowledge Dr. Richard Frayne for his assistance with MRI sequence development and image acquisition.

Disclosure statement

The authors have no financial or personal relationships with other people or organizations that could innapropriately influence this work.

Funding

This work was supported by the Natural Sciences and Engineering Research Council of Canada (NSERC), Alberta Innovates Technology Futures (AITF), the Canadian Institutes of Health Research (CIHR), and Alberta Innovates Health Solutions (AIHS).

References

Blankevoort L, Huiskes R, de Lange A. 1988. The envelope of passive knee joint motion. J Biomech. 21:705–720.

Blankevoort L, Huiskes R, de Lange A. 1990. Helical axes of passive knee joint motions. J Biomech. 23:1219–1229.

Churchill DL, Incavo SJ, Johnson CC, Beynnon BD. 1998. The transepicondylar axis approximates the optimal flexion axis of the knee. Clin Orthop Relat Res: 111–118.

Cole GK, Nigg BM, Ronsky JL, Yeadon MR. 1993. Application of the joint coordinate system to three-dimensional joint attitude and movement representation: a standardization proposal. J Biomech Eng. 115:344–349.

Colle F, Bignozzi S, Lopomo N, Zaffagnini S, Sun L, Marcacci M. 2012. Knee functional flexion axis in osteoarthritic patients: comparison *in vivo* with transepicondylar axis using a navigation system. Knee surgery, Sport Traumatol Arthrosc. 20:552–558.

Coughlin KM, Incavo SJ, Churchill DL, Beynnon BD. 2003. Tibial axis and patellar position relative to the femoral epicondylar axis during squatting. J Arthroplasty. 18:1048–1055.

Dennis DA, Mahfouz MR, Komistek RD, Hoff W. 2005. In vivo determination of normal and anterior cruciate ligament-deficient knee kinematics. J Biomech. 38:241–253.

Dhaher YY, Francis MJ. 2006. Determination of the abduction–adduction axis of rotation at the human knee: helical axis representation. J Orthop Res. 24:2187–2200.

Fleming BC, Beynnon BD, Tohyama H, Johnson RJ, Nichols CE, Renstrom P, Pope MH. 1994. Determination of a zero strain reference for the anteromedial band. J Orthop Res. 12:789–795.

Freeman MAR, Pinskerova V. 2005. The movement of the normal tibio-femoral joint. J Biomech. 38:197–208.

Grip H, Häger C. 2013. A new approach to measure functional stability of the knee based on changes in knee axis orientation. J Biomech. 46:855–862.

Grood ES, Suntay WJ. 1983. A joint coordinate system for the clinical description of three-dimensional motions: application to the knee. J Biomech Eng. 105:136–144.

Iwaki H, Pinskerova V, Freeman MAR. 2000. Tibiofemoral movement 1: the shapes and relative movements of the femur and tibia in the unloaded cadaver knee. J Bone Jt Surg. 82:1189–1195.

Jonsson H, Kärrholm J. 1994. Three-dimensional knee joint movements during a step-up: Evaluation after anterior cruciate ligament rupture. J Orthop Res. 12:769–779.

Kessler O, Durselen L, Banks S, Mannel H, Marin F. 2007. Sagittal curvature of total knee replacements predicts *in vivo* kinematics. Clin Biomech. 22:52–58.

Küpper JC, Robu I, Frayne R, Ronsky JL. 2013. The knee loading apparatus: axial, anterior, and compressive loading with magnetic resonance imaging. J Mech Des. 135:024501.

Morishige M, McQueen DA, Chong A, Ballard GP, Cooke FW. 2010. The influence of sequential debridement in total knee arthroplasty on the flexion axis of the knee using computer-aided navigation. J Orthop Res. 28:767–772.

Peters A, Galna B, Sangeux M, Morris M, Baker R. 2010. Quantification of soft tissue artifact in lower limb human motion analysis: A systematic review. Gait & Posture. 31(1):1–8.

Sakane M, Livesay GA, Fox RJ, Rudy TW, Runco TJ, Woo SL-Y. 1999. Relative contribution of the ACL, MCL, and bony contact to the anterior stability of the knee. Knee surgery, Sport Traumatol Arthrosc. 7:93–97.

Sheehan FT. 2007. The finite helical axis of the knee joint (a non-invasive *in vivo* study using fast-PC MRI). J Biomech. 40:1038–1047.

Shiavi R, Limbird T, Frazer M, Stivers K, Strauss A, Abramovtiz J. 1987. Helical motion analysis of the knee – I. Methodology for studying kinematics during locomotion. J Biomech. 20:459–469.

Soderkvist I, Wedin P. 1993. Determining the movements of the skeleton using well-configured markers. J Biomech. 26:1473–1477.

Spoor CW, Veldpaus FE. 1980. Rigid body motion calculated from spatial co-ordinates of markers. J Biomech. 13:391–393.

Van den Bogert A, Read L, Nigg BM. 1996. A method for inverse dynamic analysis using accelerometry. J Biomech. 29:949–954.

Van den Bogert AJ, Reinshmidt C, Lundberg A. 2008. Helical axes of skeletal knee joint motion during running. J Biomech. 41:1632–1638.

Westphal CJ, Schmitz A, Reeder SB, Thelen DG. 2013. Load-dependent variations in knee kinematics measured with dynamic MRI. J Biomech. 46:2045–2052.

Woltring HJ, Huiskes R, de Lange A, Veldpaus FE. 1985. Finite centroid and helical axis estimation from noisy landmark measurements in the study of human joint kinematics. J Biomech. 18:379–389.